



## Research Paper

# Hypoxic acclimation improves cardiac redox homeostasis and protects heart against ischemia-reperfusion injury through upregulation of O-GlcNAcylation

Wei Ou<sup>a,b,c,1</sup>, Yu Liang<sup>a,b,1</sup>, Yu Qin<sup>d,1</sup>, Wei Wu<sup>d,1</sup>, Maodi Xie<sup>a,b</sup>, Yabing Zhang<sup>a,b</sup>, Yarong Zhang<sup>e</sup>, Liwei Ji<sup>a,b</sup>, Haiyang Yu<sup>e</sup>, Tao Li<sup>a,b,\*</sup>

<sup>a</sup> Laboratory of Mitochondria and Metabolism, Department of Anesthesiology, National Clinical Research Center for Geriatrics, West China Hospital of Sichuan University, Chengdu, 610041, China

<sup>b</sup> Laboratory of Anesthesia and Critical Care Medicine, West China Hospital of Sichuan University, Chengdu, 610041, China

<sup>c</sup> Department of Anesthesiology, Nanchong Central Hospital, Nanchong, 637000, China

<sup>d</sup> Department of Anesthesiology, The General Hospital of Western Theater Command, Chengdu, 610083, China

<sup>e</sup> State Key Laboratory of Oral Diseases, National Clinical Research Center for Oral Diseases, West China Hospital of Stomatology, Sichuan University, Chengdu, 610041, China



## ARTICLE INFO

## Keywords:

Hypoxia  
Ischemia-reperfusion injury  
Heart  
Redox homeostasis  
Glucose metabolism  
Mitochondria

## ABSTRACT

Ischemia-reperfusion (I/R) injury is detrimental to cardiovascular system. Alteration in glucose metabolism has been recognized as an important adaptive response under hypoxic conditions. However, the biological benefits underlying this metabolic phenotype remain to be elucidated. This study was designed to investigate the impact of hypoxic acclimation (HA) on cardiac I/R injury and the antioxidative mechanism(s). Male adult mice were acclimated in a hypoxic chamber (10% oxygen [O<sub>2</sub>]) for 8 h/day for 14 days, and then subjected to cardiac I/R injury by ligation of left anterior descending coronary artery for 30 min and reperfusion for 24 h or 7 days. Our results showed that HA attenuated oxidative stress and reduced infarct size in the I/R hearts. This cardioprotective effect is coupled with an elevation of protein O-linked N-acetylglucosamine (O-GlcNAc) modification partially due to inflammatory stimulation. Hyperglycosylation activated glucose-6-phosphate dehydrogenase (G6PDH), the rate-limiting enzyme in the pentose phosphate pathway, resulting in an upregulation of NADPH/NADP<sup>+</sup> and GSH/GSSG couples and enhancement of redox homeostasis in the heart. Pharmacological suppression of O-GlcNAcylation totally abolished the influence of HA on the G6PDH activity, redox balance and post-I/R damage in the hearts and cultured cardiomyocytes, whereby augmentation of O-GlcNAcylation further enhanced the benefits, suggesting a central role of O-GlcNAcylation in HA-initiated antioxidative and cardioprotective effects. These findings, therefore, identified HA as a promising anti-I/R strategy for the heart and proposed O-GlcNAc modification of G6PDH as a therapeutic target in ischemic heart disease.

## 1. Introduction

The cardiovascular system is a vulnerable target for ischemia-reperfusion (I/R) injury, which leads to irreversible cardiac dysfunction and damage [1,2]. Modern lifestyle and unhealthy dietary habits raise the prevalence of atherosclerotic vascular disease and increase the risk of I/R injury in the heart. I/R injury contributes to the pathogenesis of multiple cardiac diseases, including infarction, arrhythmias, hypertrophy and heart failure [3,4]. The latest epidemiological data show that

cardiovascular diseases take the lives of 17.9 million people every year, and this number is expected to increase to more than 23.6 million by 2030, standing as a major cause of morbidity and mortality worldwide [5]. Moreover, I/R injury is the leading cause of death and poor prognosis of patients in cardiac surgery and heart transplantation. The threat will likely increase as the population continues to age and the elderly people are more sensitive to I/R insults. Thus, strategies that can increase the resistance of heart to I/R injury are urgently required.

Several lines of evidence point to the existence of endogenous coping

\* Corresponding author. West China Hospital, Sichuan University No 37 Wainan Guoxue Road, Chengdu, Sichuan 610041, China.

E-mail address: [scutaoli1981@scu.edu.cn](mailto:scutaoli1981@scu.edu.cn) (T. Li).

<sup>1</sup> The first four authors contributed equally to this study.

<https://doi.org/10.1016/j.redox.2021.101994>

Received 10 February 2021; Received in revised form 11 April 2021; Accepted 22 April 2021

Available online 30 April 2021

2213-2317/© 2021 The Author(s).

Published by Elsevier B.V. This is an open access article under the CC BY-NC-ND license

(<http://creativecommons.org/licenses/by-nc-nd/4.0/>).

mechanisms for dealing with I/R injury [6]. Release of extracellular signaling molecules such as adenosine, bradykinin and opioids, activation of protein kinase C and classic PI3K/Akt/MEK1/2/ERK1/2 cascades, as well as mild production of reactive oxygen species (ROS) are reported to contribute to the protective hypoxic response [7–10]. Through these mechanisms, ischemic preconditioning has been widely accepted as a powerful and reproducible remedy for cardioprotection [11–13]. Compared to restriction of blood flow in the heart, regulation of blood oxygen level via hypoxia is more practicable [10]. However, the outcomes from chronic hypoxia exposure or hypoxic acclimation (HA) are complicated. It is believed to improve exercise capacity [14], raise maximal oxygen ( $O_2$ ) consumption [15], protect I/R hearts [16,17], and have therapeutic potential for mitochondrial disease [18]. On the contrary, chronic hypoxia, in particular, intermittent hypoxia is reported to cause pulmonary hypertension and impair neuropsychological function, in patients with chronic obstructive pulmonary disease and in healthy people at high altitude [15]. The molecular mechanisms by which hypoxia exposure mediates these seemingly contradictory effects, however, remain elusive.

Glycolysis is a cytoplasmic pathway that breaks down glucose into pyruvate and lactate, with net generation of 2 molecules of ATP in the absence of  $O_2$ . More importantly, it has been established that glycolysis is intimately related to redox biology [19]. Under physiological conditions, glycolysis controls the nicotinamide adenine dinucleotide redox couple ( $NADH/NAD^+$ ), and provides the major reductant, nicotinamide adenine dinucleotide phosphate (NADPH) for thiol-dependent antioxidant defenses. Thus, alteration in glucose metabolism has been recognized as an important adaptive response under hypoxic conditions. Nonetheless, the metabolic phenotype and redox status, as well as the biological impact underlying HA have not been fully understood.

In the present study, we sought to identify the impact of HA on cardiac I/R injury and to elucidate underlying mechanisms. Our results demonstrated that the HA-exposed hearts have elevated protein O-GlcNAcylation, enhanced pentose phosphate pathway (PPP) and improved redox homeostasis, which mitigate cardiac I/R injury.

## 2. Materials and methods

### 2.1. Mice

All animal experiments were performed with the approval of the Institutional Animal Care and Use Committee of the West China Hospital, Sichuan University, China. The animals received humane care in compliance with the *Guide for the Care and Use of Laboratory Animals* published by NIH. Male C57BL/6J mice, 8–10 weeks old, were purchased from Huafukang Experimental Animal Center, China. Mice were maintained in a vivarium with a 12-h light/dark cycle at 22 °C and free access to food and water. To modulate cardiac protein O-GlcNAcylation level, mice were treated by intraperitoneal injection with alloxan (ALX, 100 mg/kg; Sigma) or Thiamet-G (TMG, 20 mg/kg; MCE) at 6 h before cardiac I/R surgery. Before injection, ALX or TMG was dissolved in saline (vehicle).

### 2.2. Cell culture

The H9c2 rat cardiomyocytes were obtained from the American Type Culture Collection (ATCC; Rockville, MD, USA). Cells were cultured in Dulbecco's modified Eagles's medium (DMEM; HyClone) containing 1 g/L glucose, 4 mM glutamine, 110 mg/L sodium pyruvate, 10% (v/v) fetal bovine serum, 100 U/ml penicillin and 100 mg/ml streptomycin (HyClone) under a humidified atmosphere containing 5% carbon dioxide ( $CO_2$ ) at 37 °C. To test the effect of inflammatory stimulation on protein O-GlcNAcylation, the H9c2 cells were treated by interleukin (IL)-1 $\beta$  (#HY-P7097A, MCE) and IL-6 (#HY-P7103A, MCE) for 4 or 24 h. To validate this effect, the H9c2 cells were incubated with LMT28 (30  $\mu$ M; #HY-102084, MCE) or neutralizing antibodies for IL-1 $\beta$  (20  $\mu$ g/ml;

#BE0246, BioXCell) or IL-6 (20  $\mu$ g/ml; #BE0046, BioXCell) during HA. To attenuate protein O-GlcNAcylation, the H9c2 cells were exposed to 6-Diazo-5-oxo-L-nor-Leucine (DON, 20  $\mu$ M; MCE) for 24 h.

### 2.3. HA exposure

To perform HA, the mice were placed in a transparent, semi-opened chamber ventilated with room air or 10%  $O_2$  at a flow rate of 18 L/min, for 8 h/day (from 9:00 a.m. to 17:00 p.m.) for 14 days. The chamber was maintained at a temperature of 22–24 °C and a humidity of 40–50%. An  $O_2$  sensor (AR8100S, Smart Sensor, China) was used to continuously monitor the  $O_2$  concentration in the chamber. Two small silent fans were placed inside the HA chamber to facilitate the removal of  $CO_2$ . For the cell culture study, the H9c2 cells were incubated under hypoxia environment (10%  $O_2$ , 5%  $CO_2$  and 85% $N_2$ ) for 8 h/day and then switched to normoxia (20%  $O_2$ , 5%  $CO_2$  and 75% $N_2$ ) for 16 h/day, and this treatment was repeated for 4 days.

### 2.4. Mouse model of cardiac I/R injury

Myocardial I/R injury was induced by ligation of left anterior descending coronary artery (LAD) for 30 min and reperfusion for 24 h or 7 days as previously described [20,21]. Briefly, mice were anesthetized by intraperitoneal injection of ketamine (120 mg/kg) and xylazine (4 mg/kg), intubated and ventilated with pure  $O_2$ , using a MiniVent mouse ventilator (Model 845, Harvard Apparatus). Body temperature was kept at 35–36 °C with a temperature controlled surgical pad. After a left thoracotomy was performed through the fifth intercostal space, the LAD was ligated with a 6-0 silk suture for 30 min of ischemia. Reperfusion was accomplished by releasing the slipknot and the chest was closed in layers. After 24 h or 7 days of reperfusion, mice were sacrificed for analysis.

### 2.5. Determination of infarct size

I/R induced myocardial infarction was determined by Evans blue and tetrazolium chloride (TTC) double staining as described previously [22]. Briefly, after 24 h of reperfusion, the ligature around the LAD was retied and the heart was quickly excised and mounted on a Langendorff apparatus. After washing out the blood by saline, 0.2 ml 1% Evans blue dye was injected through aortic root. The hearts were sliced transversally into 1-mm-thick sections and 5–6 sections per heart starting from the apex. The sections were incubated in 1% TTC in PBS at 37 °C for 15 min and then fixed in a 4% paraformaldehyde solution for 24 h at room temperature. The area at risk (AAR) was identified by the absence of blue dye. The total LV area, AAR and TTC-negative staining area (infarcted myocardium) were measured with Image J software (NIH). Myocardial infarction was expressed as a percentage of the infarct size (IS) over AAR (IS/AAR) and the size of AAR was expressed as the percentage of AAR over total LV area.

### 2.6. Measurement of creatine kinase-MB (CK-MB)

After 24 h of reperfusion, blood samples were taken by heart puncture and plasma samples were collected by centrifuge at 2500 rpm for 10 min. The levels of CK-MB in plasma were detected by a biochemical analyzer (BS-120, Mindray, China).

### 2.7. Histological assessment

Hearts were arrested in diastole by KCl (30 mM), perfusion fixed with 10% neutral buffered formalin, paraffin embedded and cut into 5- $\mu$ m-thick sections. For hematoxylin and eosin (H&E) staining, the sections were stained with hematoxylin for 8 min and eosin for 1 min, washed in 0.5% hydrochloric acid alcohol, dehydrated and mounted. For the Masson's trichrome staining, all the heart samples were sectioned into 5

$\mu\text{m}$  slices starting from the suture ligation site to the apex, and every 50th slices were reserved for staining. Sections were stained using a commercially available kit (#G1340, Solarbio, China) for quantification of the scar size in the heart [23]. All sections were imaged through a fluorescence microscope (AX10 imager A2/AX10 cam HRC, Zeiss).

## 2.8. ROS and superoxide production assays

As markers of oxidative stress, the superoxide dismutase (SOD) activity and malondialdehyde (MDA) formation in cardiac tissues were measured by using commercially available kits (Beyotime, China). For dihydroethidine (DHE) staining, mouse cardiac tissues were embedded in Tissue-Tek OCT (Thermo Fisher). Cryosections (10  $\mu\text{m}$ ) were incubated with superoxide-sensitive dye DHE (10  $\mu\text{M}$  in 0.01% DMSO) at 37 °C for 30 min in a humidified dark chamber. Red DHE fluorescence was detected with an Olympus IX83 microscope (Olympus) at room temperature. The levels of protein carbonylation in cardiac tissues were detected by using the OxyBlot protein oxidation detection kit (Sigma-Aldrich). For measurement of mitochondrial superoxide production, the H9c2 cells were incubated with MitoSOX Red (2.5  $\mu\text{M}$ ; Thermo Fisher) at 37 °C for 30 min, washed with PBS and resuspended in 200  $\mu\text{l}$  cold PBS for flow cytometry analysis (Ex/Em: 510nm/580 nm; Beckman Coulter cytoFLEX, USA). For the evaluation of intracellular oxidative stress, cells were incubated with CM-H2DCFDA (10  $\mu\text{M}$ ; #HY-D0940, MCE) at 37 °C for 30 min. Fluorescence intensity was quantified by a flow cytometer (Ex/Em: 488nm/525 nm; Beckman Coulter cytoFLEX, USA) [24]. The oxidative DNA damage was also assessed as reported [25]. Briefly, H9c2 cells were fixed with 4% paraformaldehyde and permeabilized with 0.1% Triton X-100. After blocking at room temperature for 1 h, H9c2 cells were incubated with anti-7,8-dihydro-8-oxo-2'-deoxyguanosine (8-Oxo-dG; #BS-1278R, Bioss, MA) and anti-TOM20 (#66777-1-Ig, Proteintech, China) at 4 °C overnight, followed by incubation with anti-mouse-IgG Alexa 488 (#ab150113, Abcam) and anti-rat-IgG Alexa 647 (#ab150075, Abcam) secondary antibodies. Before imaged by a confocal microscope (CLSM, FV3000, Olympus, Japan), the cells were stained with 4',6-diamidino-2-phenylindole (DAPI; #D9542, Sigma). Fifty randomly chosen cells from each group were analyzed through Image J software, and fluorescence intensities in nuclei and mitochondria were assessed respectively for each condition.

## 2.9. Transmission electron microscopy

The cardiac tissues were fixed for 24 h in 3% glutaraldehyde in 0.1 M phosphate buffer saline (pH 7.4), and then fixed with 1% osmium tetroxide for 1 h. After the samples were dehydrated in a series of ethanol and were embedded in Epon 812, ultrathin sections were prepared and counterstained with uranyl acetate and lead citrate. The stained sections were examined under a transmission electron microscope (JEM-1400PLUS, JEOL, Japan). The images were assessed in a blinded fashion by pathologists.

## 2.10. Apoptosis analysis

Apoptosis was measured by Annexin V and propidium iodide (PI) dual staining according to the manufacturer's instruction (4A Biotech, China). Briefly, H9c2 cells were incubated with 5  $\mu\text{l}$  Annexin V-FITC for 5 min at room temperature in the dark, and then added 10  $\mu\text{l}$  PI. The apoptosis rate was determined by flow cytometry analysis (Annexin V-FITC, Ex/Em: 488nm/525 nm; PI, Ex/Em: 561nm/575 nm).

## 2.11. Glucose uptake assay

The H9c2 cells were cultured in 96-well plates (5000 cells/well). After treatment with IL-1 $\beta$  (5 ng/ml) or IL-6 (5 ng/ml) for 24 h, the cells were incubated with a fluorescent glucose analog 2-[N-(7-nitrobenz-2-oxa-1,3-diazol-4-yl) amino]-2-deoxyglucose (2-NBDG, 300  $\mu\text{M}$ ; Cayman

Chemical) in glucose-free DMEM for 40 min at 37 °C in the dark. After washing off excessive fluorescent dye, fluorescence intensities were measured by a plate reader (Synergy MX, BioTek Instruments).

## 2.12. Western blotting and immunoprecipitation

Frozen myocardial tissue or cultured cells were lysed with ice-cold RIPA lysis buffer with protease inhibitor cocktail, and then centrifuged at 13000g for 15 min at 4 °C. Protein extracts were separated by SDS-PAGE and transferred to PVDF membranes. Membrane was blocked in 5% non-fat milk and incubated with primary antibodies at 4 °C overnight, including anti-O-GlcNAc (#ab2739, Abcam), anti-OGT (#11576-2-AP, Proteintech, China), anti-OGA (#14711-1-AP, Proteintech), anti-GFAT1 (#14132-1-AP, Proteintech), anti-GALE (#14414-1-AP, Proteintech), anti-HK2 (#22029-1-AP, Proteintech), anti-IL-1 $\beta$  (#AF4006, Affbiotech, China), anti-IL-6 (#DF6087, Affbiotech), anti-G6PDH (#DF6444, Affbiotech), anti-GAPDH (#10494-1-AP, Proteintech), anti-Tubulin (#11224-1-AP, Proteintech) and anti- $\beta$ -actin (#20536-1-AP, Proteintech) antibodies. After incubation with HRP conjugated secondary antibodies (#SA00001-1 and #SA00001-2, Proteintech), the signal intensities were visualized by an ECL Western blot detection kit (#P10100, ECM) and quantified by Image J software (NIH).

For immunoprecipitation experiments, tissue or cell lysates were incubated with anti-O-GlcNAc antibody or control immunoglobulin (IgG, Proteintech) overnight. Antibody-bound proteins were precipitated with protein G magnetic beads (#1614023; Bio-Rad) and washed three times with lysis buffer. Samples were prepared for further analysis by Western blotting.

## 2.13. O-glycoproteomics analysis

Cardiac tissues were lysed in native lysis buffer (Solarbio Life Sciences) supplemented with complete protease inhibitor cocktail (Roche), PMSF and Na<sub>2</sub>VO<sub>3</sub>. The lysates were incubated with anti-O-GlcNAc (#ab2739, Abcam) antibody at 4 °C overnight. Antibody-bound proteins were precipitated with protein G magnetic beads (#1614023, Bio-Rad) and washed three times with lysis buffer. Enriched O-GlcNAc peptide samples were dissolved and loaded for LC separation on a NanoElute UHPLC system (Bruker Daltonics). Enriched peptides were analyzed on a timsTOF Pro mass spectrometer (Bruker Daltonics), equipped a ReproSil-Pur Basic C18 column. All mass spectrometric data were searched with Maxquant (v 1.6.1.0) and against Uniprot Mus\_musculus\_10090 database concatenated with reverse decoy database. Label free MS<sup>1</sup> based quantification of peptides was performed using Mass-ChroQ. Retention time alignment between LC-MS data files was performed using the obiwrap method. The HA/Control ratio of each O-GlcNAc peptide was estimated by the average value of 3 hearts in each group, and the ratio >1.5 was define as hyperglycosylated. Gene Ontology (GO) annotation proteome was derived from the UniProt-GOA database (<http://www.ebi.ac.uk/GOA/>).

## 2.14. Determination of glucose-6-phosphate dehydrogenase (G6PDH) activity and related redox couples

The G6PDH activity, reduced nicotinamide adenine dinucleotide phosphate/nicotinamide adenine dinucleotide phosphate (NADPH/NADP<sup>+</sup>) ratio and glutathione/glutathione disulfide (GSH/GSSG) ratio in cardiac tissues and cultured cells were determined by commercial kits according to the manufacturer's protocols (Beyotime, China).

## 2.15. Measurement of mitochondrial oxygen consumption rate (OCR)

Mitochondria from cardiac tissue were isolated by differential centrifugation as described previously [26]. The OCRs of isolated intact mitochondria or H9c2 cells were measured with a Seahorse XFe24 analyzer (Agilent Technologies, Santa Clara, CA). Freshly isolated

cardiac mitochondria or H9c2 cells were transferred to a XFe24 microplate, and the microplate were filled with Mitochondrial Assay Solution (MAS: 220 mM mannitol, 70 mM sucrose, 10 mM MgCl<sub>2</sub>, 2 mM HEPES, 1 mM EGTA, 10 mM KH<sub>2</sub>PO<sub>4</sub> and BSA 0.02% (w/v) at pH 7.2) to a final amount of 500  $\mu$ l containing succinate (10  $\mu$ M; Sigma). The OCR was measured in response to sequential injection of ADP (4 mM; Sigma), oligomycin (2.5  $\mu$ g/ml; MCE), trifluorocarbonyl cyanide phenylhydrazine (FCCP, 4  $\mu$ M; MCE), and antimycin A (4  $\mu$ M; Sigma), at 37 °C. The respiratory rates are reported as oxygen flux per mass, and all readings are normalized to  $\mu$ g of mitochondrial protein or cell numbers (pmol O<sub>2</sub>/min/ $\mu$ g protein or 25000 cells).

## 2.16. Statistical analysis

Statistical analysis was performed using GraphPad Prism v.8.0.1 (GraphPad, La Jolla, CA). Shapiro-Wilk Normality test was performed to determine data distribution. All data are normally distributed and presented as mean  $\pm$  SEM. Unpaired 2-tailed Student *t*-test was used to compare 2 groups, and one-way ANOVA followed by Tukey's multiple comparisons test was performed to determine differences among >2 groups. A simple linear regression analysis was performed to estimate the correlation between protein O-GlcNAcylation and proinflammatory cytokines IL-1 $\beta$  and IL-6. *P* values < 0.05 were considered statistically significant.

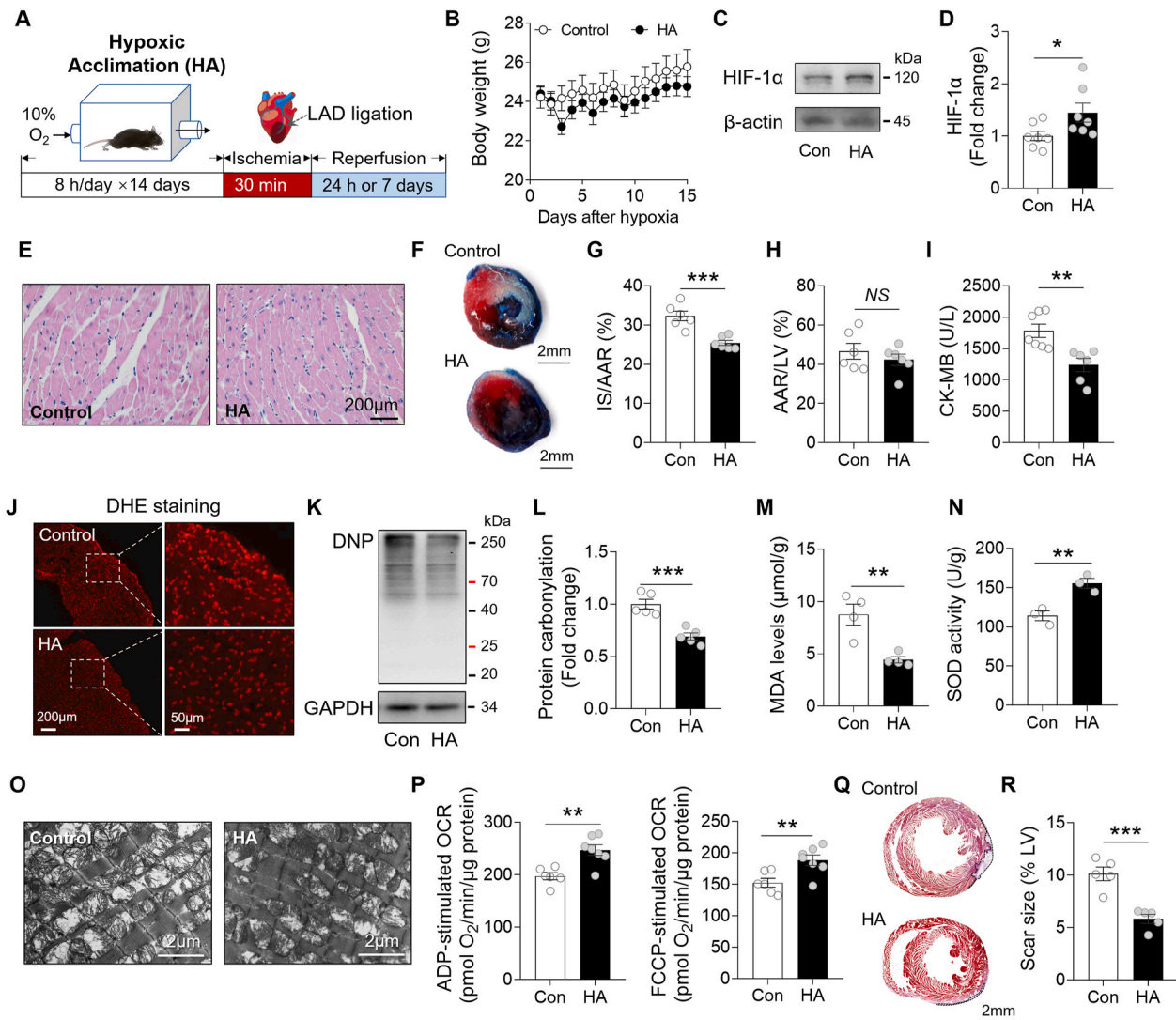


**Fig. 1.** HA attenuated cardiac infarction and oxidative stress after I/R injury. **A**, A schematic representation of the experimental protocol. **B**, The body weight of the Control and HA mice (*n* = 15 per group). **C-D**, Immunoblot analysis of HIF-1 $\alpha$  in the Control and HA hearts (*n* = 7 per group). **E**, Representative images of Hematoxylin and Eosin (H&E)-stained left ventricle (LV) tissue sections (*n* = 5 per group). Scale bar, 200  $\mu$ m. **F**, Representative images of Evans blue and tetrazolium chloride (TTC) double-stained heart sections. Blue represents unaffected, viable tissue. White represents infarct area. Red + white represents area at risk. Scale bar, 2 mm. **G-H**, Quantifications of infarct size (IS) relative to area at risk (AAR) (**G**) and AAR relative to LV (**H**) (*n* = 6 per group). **I**, The levels of CK-MB in plasma (Control: *n* = 7, HA: *n* = 6). **J**, Representative images for Dihydroethidium (DHE) staining (*n* = 50 fields, from 5 hearts/group). Scale bar, 200  $\mu$ m or 50  $\mu$ m. **K-L**, Representative immunoblots of protein carbonylation in the LV ischemic border zone (**K**). Protein carbonyls was derivatized to 2,4-dinitrophenylhydrazine (DNP) and then probed with antibody for DNP. Quantification of band intensity (**L**). The DNP levels of derivatized proteins were normalized by GAPDH and data were expressed as fold change relative to Control (*n* = 5 per group). **M**, MDA levels in cardiac tissues (*n* = 4 per group). **N**, SOD activity in cardiac tissues (*n* = 4 per group). **O**, Representative electron microscopy images of the Control and HA heart sections (*n* = 5 per group). Scale bar, 2  $\mu$ m. **P**, The ADP- and FCCP-stimulated oxygen consumption rates (OCR) in the presence of succinate of the isolated mitochondria from the mouse hearts (Control: *n* = 6, HA: *n* = 7). **Q**, Representative images of Masson's trichrome-stained heart sections 7 days post-I/R. **R**, Quantification of the scar size relative to left ventricle (*n* = 5 per group). Scale bar, 2 mm. Dotted line indicates the scar area. Data are shown as mean  $\pm$  SEM. \**P* < 0.05, \*\**P* < 0.01 and \*\*\**P* < 0.001 for indicated comparisons. NS: no significant difference. (For interpretation of the references to colour in this figure legend, the reader is referred to the Web version of this article.)

### 3. Results

#### 3.1. HA attenuated cardiac infarction and oxidative stress after I/R injury

To perform HA, mice were exposed to 10% O<sub>2</sub> environment for 8 h per day for 14 days (Fig. 1A). The mice showed normal gain of body weight during treatment (Fig. 1B), while the expression of HIF-1 $\alpha$  in the heart was significantly elevated as compared to the Control group, suggesting that HA activated cardiac hypoxia signaling without perturbation of growth (Fig. 1C and D). H&E staining showed no histologic changes in hearts between Control and HA groups (Fig. 1E). To understand the functional impact of HA on heart, the mice were subjected to cardiac I/R injury through LAD ligation. A lower infarct size was observed in HA hearts at 24 h after I/R (Fig. 1F–H), accompanied by a downregulated release of cardiac enzyme CK-MB in plasma (Fig. 1I). It has been well established that oxidative stress is a hallmark of I/R injury and contributes to post-I/R pathogenesis, we thus investigated whether the benefit from HA was mediated by suppression of oxidative stress. After 24 h of I/R injury, the fluorescence intensity of DHE-stained cardiac tissue was decreased in the HA group, indicating a lower level of ROS production (Fig. 1J). Moreover, we observed attenuated protein carbonylation, an irreversible oxidative protein modification, and reduced levels of MDA, a marker of lipid peroxidation, as well as an increased SOD activity in the HA hearts (Fig. 1K–N). Mitochondrion is extremely sensitive to oxidative stress. Along with reduced oxidation stress, the mitochondrial morphology in cardiac tissue at border zone was preserved by HA; the disorganized cristae and reduced matrix density induced by I/R injury were largely alleviated (Figure 1O). Seahorse analysis showed that the mitochondrial respiratory function was also improved by HA (Figure 1P). To understand whether these protective effects bring a long-term benefit on the I/R heart, we analyzed the scar size by Masson's trichrome staining at 7 days after I/R, and found it was remarkably reduced in the HA group (Fig. 1Q–R). Taken

together, these results suggest that HA exposure limited infarct scar and reduced oxidative stress in hearts after I/R injury.

#### 3.2. HA promoted protein O-GlcNAcylation in I/R hearts

Accumulating evidence suggest that the status of protein glycosylation modulates the response of heart to I/R injury [26–28]. We observed an ~60% increase in protein O-linked *N*-acetylglucosamine (O-GlcNAc) modification in the HA heart after I/R (Fig. 2A). This increase was accompanied by an enhancement of hexosamine biosynthetic pathway (HBP), a branch of glycolytic pathway (Fig. 2B). The protein abundance of UDP-galactose 4'-epimerase (GALE), the enzyme responsible for interconversion of UDP-*N*-acetylglucosamine (UDP-GlcNAc) and UDP-*N*-acetylgalactosamine (UDP-GalNAc), was greatly elevated by HA. Also, the protein levels of O-GlcNAc transferase (OGT) and hexokinase 2 (HK2), which conjugates O-GlcNAc groups to target protein or generates glucosamine-6-phosphate (GlcN-6-P) from glucosamine, respectively, were also upregulated (Fig. 2C). Furthermore, the glucose tolerance test showed that HA improved the uptake of glucose in circulation, which may satisfy the carbohydrate demand for the enhanced HBP flux (Fig. 2D and E). Together, the data suggest that the cardioprotective effect of HA is coupled with an elevation of protein O-GlcNAc modification in the heart.

#### 3.3. HA-induced inflammation stimulated protein O-GlcNAcylation in hearts

Along with the elevated O-GlcNAc modification, we found that the HA hearts increased expression of pro-inflammatory cytokines IL-1 $\beta$  and IL-6 (Fig. 3A). Similarly, upon exposure to HA condition (10% O<sub>2</sub>; 8 h/day  $\times$  4 days), the H9c2 cardiomyocytes also upregulated the expression of these cytokines (Fig. 3B). Linear regression analysis showed that the status of protein O-GlcNAcylation in the heart is positively correlated with the cardiac abundance of IL-1 $\beta$  and IL-6, suggesting a causal link

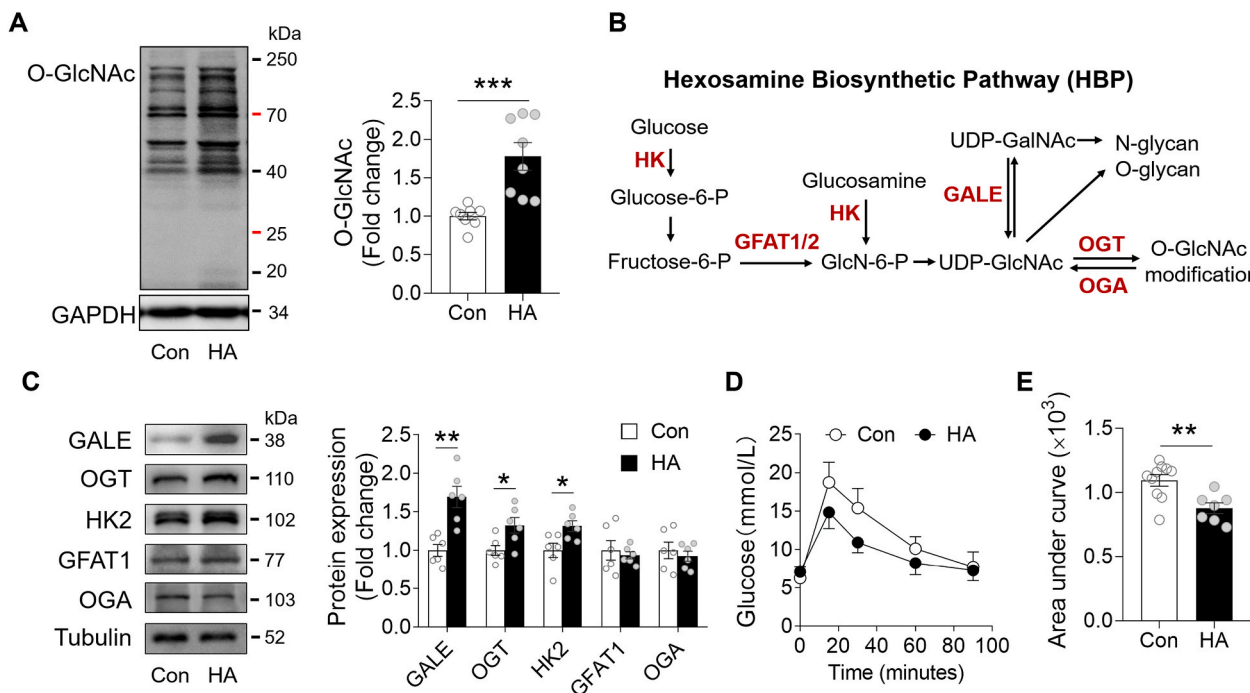


**Fig. 2.** HA promoted protein O-GlcNAcylation in I/R hearts. **A**, Immunoblot analysis of protein O-GlcNAc modification in the Control and HA hearts (n = 8 per group). **B**, The hexosamine biosynthesis pathway. HK, hexokinase. GFAT2/1, glucosamine: fructose-6-phosphate aminotransferase 2/1. GALE, UDP-glucose 4-epimerase. OGT, O-GlcNAc transferase. OGA, O-GlcNAcAcase. **C**, Immunoblot analysis of GALE, OGT, HK2, GFAT1, OGA in the Control and HA hearts (n = 6 per group). **D-E**, Glucose tolerance test of mice after 6 h of fasting (Control: n = 10, HA: n = 7). Data are shown as mean  $\pm$  SEM. \*P < 0.05, \*\*P < 0.01 and \*\*\*P < 0.001 for indicated comparisons.

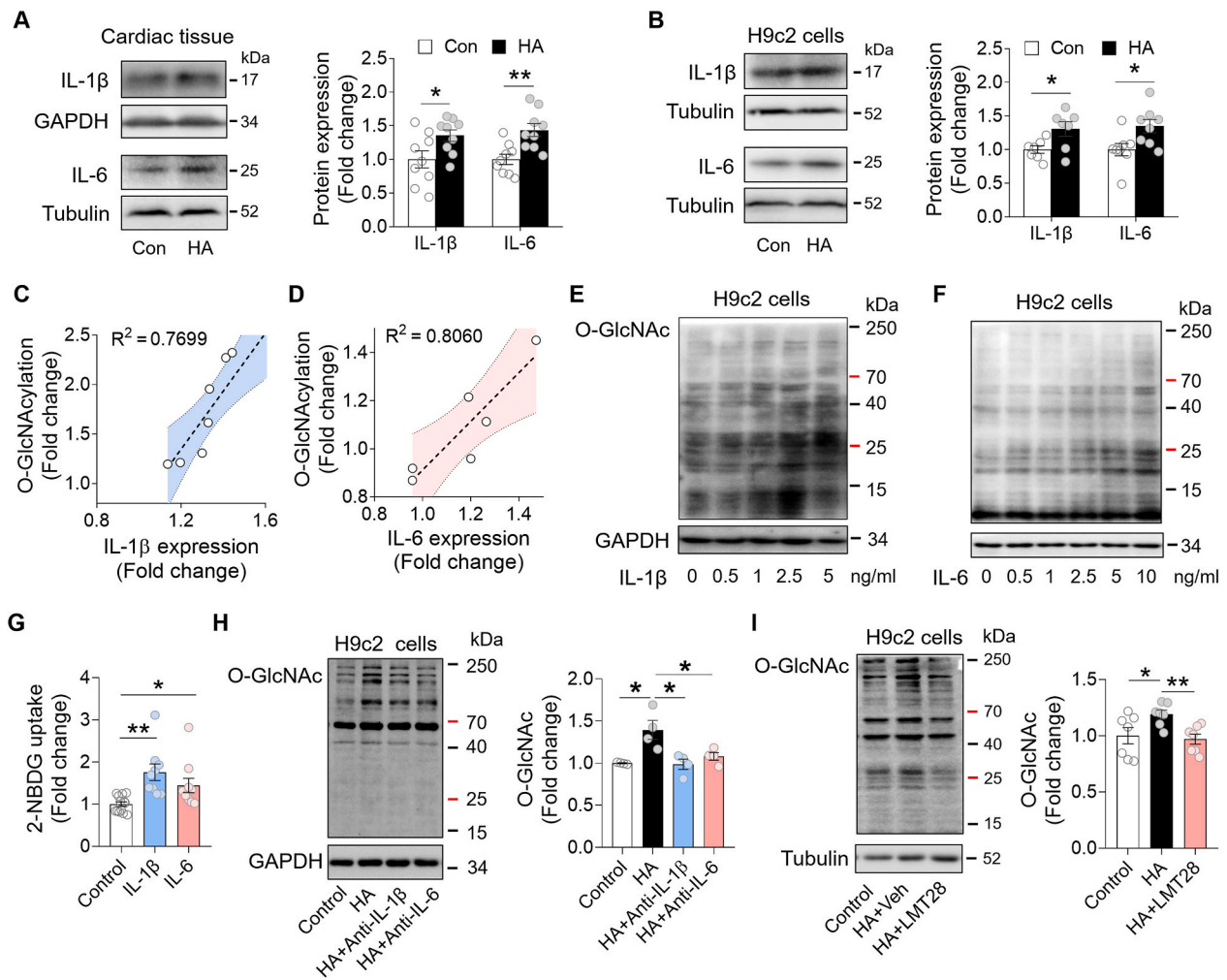


**Fig. 3.** HA-induced inflammation stimulated protein O-GlcNAcylation in hearts. **A**, Immunoblot analysis of IL-1 $\beta$  and IL-6 in the Control and HA hearts (n = 9 per group). **B**, Immunoblot analysis of IL-1 $\beta$  and IL-6 in the H9c2 cells (IL-1 $\beta$ : n = 7 per group; IL-6: n = 8 per group). **C-D**, The linear regression analysis between the expression of IL-1 $\beta$  (**C**) or IL-6 (**D**) and protein O-GlcNAcylation level. **E-F**, Representative blots of protein O-GlcNAcylation in H9c2 cells treated with increasing concentration of IL-1 $\beta$  (**E**) or IL-6 (**F**). **G**, The glucose uptake rate measure by 2-NBDG in H9c2 cells. **H**, Immunoblot analysis of protein O-GlcNAcylation in H9c2 cells after HA and neutralizing antibody treatments (n = 4 per group). **I**, Immunoblot analysis of protein O-GlcNAcylation in H9c2 cells with indicated treatments (n = 7 per group). Data are shown as mean  $\pm$  SEM. \*P < 0.05, \*\*P < 0.01 for indicated comparisons.

between HA-induced inflammation and hyperglycosylation (Fig. 3C and D). To confirm it, we incubated H9c2 cells with increasing concentration of IL-1 $\beta$  and IL-6 for 24 h. Notably, the protein O-GlcNAcylation was enhanced by both cytokines in a dose-dependent manner (Fig. 3E and F). By utilizing a glucose analog 2-NBDG, we also observed an upregulation of glucose uptake rate after IL-1 $\beta$  or IL-6 stimulation (Fig. 3G). Removal of either IL-1 $\beta$  or IL-6 by neutralizing antibodies could abrogate the effects of HA on protein O-GlcNAcylation (Fig. 3H). Interestingly, co-incubation with LMT28 during HA, a novel IL-6 inhibitor by competitive binding to IL-6 receptor, was sufficient to block HA-induced elevation of O-GlcNAcylation, indicating that IL-6-initiated downstream signaling is a potent driver in glycosylation (Fig. 3I). Taken together, these data suggested that HA-induced inflammatory cytokine secretion contributes to the elevated O-GlcNAcylation in the heart.

### 3.4. HA activated pentose phosphate pathway (PPP) via O-GlcNAcylation in hearts

To elucidate the biological impact of altered O-GlcNAcylation, we performed co-immunoprecipitation experiment with anti-O-GlcNAcylation antibody in the Control and HA hearts (Fig. 4A). Mass spectrometry

analysis identified a total of 254 proteins and 66 proteins bearing higher O-GlcNAcylation modification, and interestingly, these hyperglycosylated proteins are enriched in multiple redox related pathways including pentose phosphate shunt based on Gene Ontology (GO) annotation (Fig. 4B). As glucose-6-phosphate (G6P) generated by HK in the cytosol can be used to produce NADPH via the oxidative phase of PPP pathway, NADPH is used to reduce glutathione, a principal element of cellular antioxidant defense system (Fig. 4C) [29]. We next asked whether the enzymes and metabolites in PPP were changed by HA. The results showed that NADPH was significantly increased in HA hearts resulting in a higher NADPH/NADP<sup>+</sup> ratio (Fig. 4D and E). This shift of intracellular redox balance was associated with an elevated activity of G6P dehydrogenase (G6PDH), the rate-limiting enzyme in the PPP pathway (Fig. 4F). As expected, a significant increase of the GSH (reduced)/GSSG (oxidized) was also observed in HA hearts (Fig. 4G and H). Together, these data suggested that HA-induced glycosylation is correlated with an activation of PPP pathway, which contributes to redox homeostasis.

### 3.5. PPP was enhanced via O-GlcNAcylation-mediated activation of G6PDH

Further study showed that the total G6PDH protein expression was

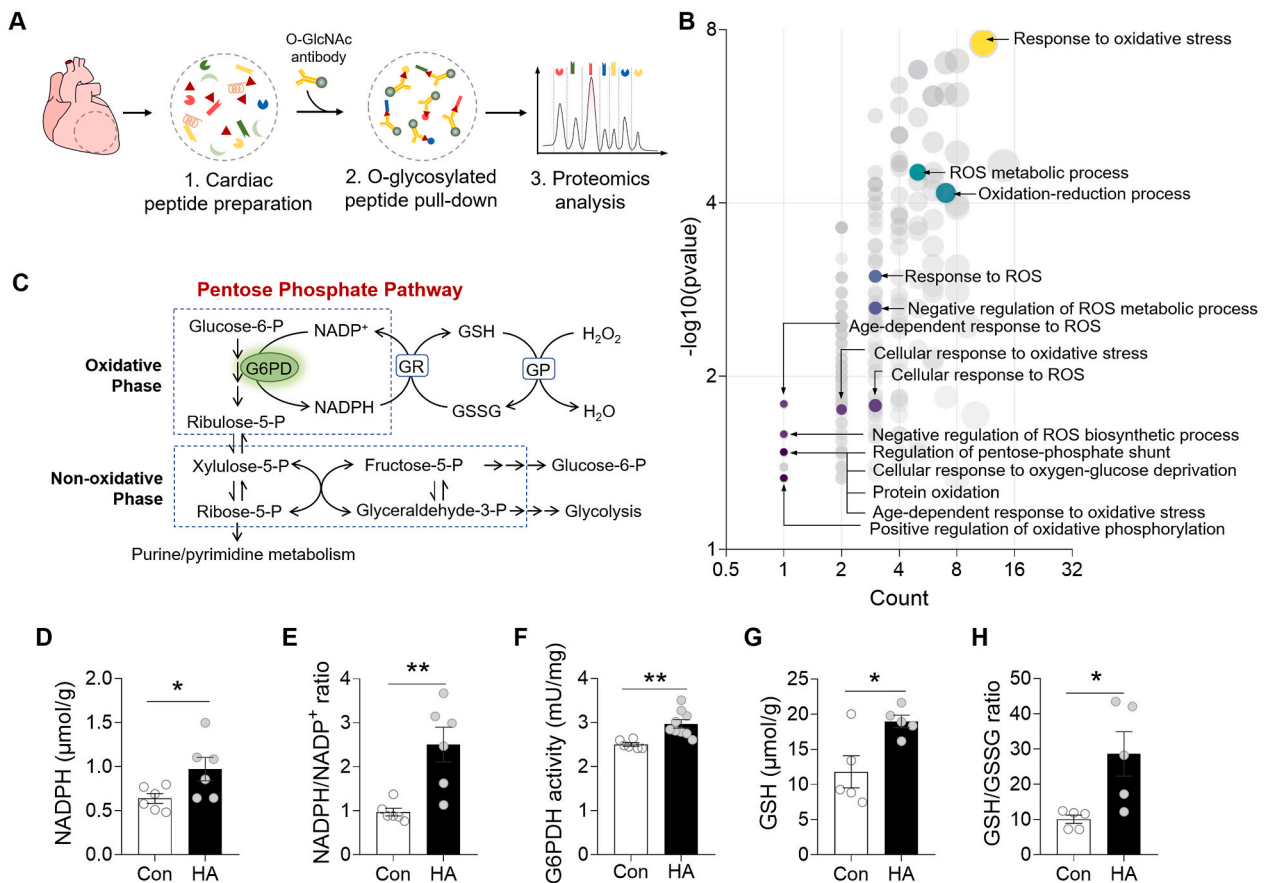


**Fig. 4.** HA activated pentose phosphate pathway (PPP) via O-GlcNAcylation in hearts. **A**, Experimental illustration of the O-glycoproteomics analysis of the Control and HA hearts. **B**, Bubble chart showing Gene Ontology (GO) annotation results. **C**, The pentose phosphate pathway. **D**, The levels of reduced nicotinamide adenine dinucleotides phosphate (NADPH) in cardiac tissue lysates ( $n = 6$  per group). **E**, The NADPH/NADP<sup>+</sup> ratio in cardiac tissue lysates ( $n = 6$  per group). **F**, The Glucose-6-phosphate dehydrogenase (G6PDH) activity in cardiac tissue lysates (Control:  $n = 6$ , HA:  $n = 9$ ). **G**, The levels of glutathione (GSH) in cardiac tissue lysates ( $n = 5$  per group). **H**, The GSH/GSSG ratio in cardiac tissue lysates ( $n = 5$  per group). Data are shown as mean  $\pm$  SEM. \* $P < 0.05$ , \*\* $P < 0.01$  for indicated comparisons.

not changed in the HA-exposed hearts and H9c2 cardiomyocytes (Fig. 5A). To understand how G6PDH was activated, we incubated the H9c2 cells with inflammatory cytokines for either 4 or 24 h, and observed that the G6PDH activity was increased only if O-GlcNAcylation level was elevated at 24 h (Fig. 5B–E). This finding ruled out the possibility that IL-1 $\beta$  and IL-6 could directly activate G6PDH in cardiomyocytes, but rather through O-GlcNAcylation. To validate it, we first treated the H9c2 cells under HA for 4 days and incubated with DON, a GFAT inhibitor for 24 h (Fig. 5F). The HA-induced and DON-suppressed O-GlcNAcylation of G6PDH in H9c2 cells was confirmed by immunoprecipitation/Western blot (IP/WB) analysis (Fig. 5G). Interestingly, HA-induced activation of G6PDH was totally abolished by DON, accompanied by a suppressed NADPH/NADP<sup>+</sup> ratio (Fig. 5H and I). Next, we treated the HA mice with ALX, an OGT inhibitor to suppress glycosylation, or TMG, a selective OGA inhibitor to further enhance it. Again, reducing O-GlcNAcylation of G6PDH by ALX lowered G6PDH activity in the HA heart, while increasing the modification by TMG further enhanced the activity (Fig. 5J and K). The elevations of redox couple NADPH/NADP<sup>+</sup> and GSH/GSSG were also attenuated by ALX but raised or maintained by TMG (Fig. 5L–M). To understand if this modulation would attenuate acute oxidative insult, the HA and DON cotreated H9c2 cells were subjected to hypoxia/reoxygenation (H/R) via oxygen glucose deprivation. After H/R, the global cellular ROS production measured using the fluorescent probe CM-H2DCFDA and oxidative DNA damage assessed by 8-Oxo-dG immunostaining were significantly reduced by HA (Fig. 6A–6C). Meanwhile, colocalization analysis indicated an >70% reduction of 8-Oxo-dG staining in mitochondria (vs

~18% in nuclei) after HA, implicating mtDNA as the likely primary target (Fig. 6B and 6C). In support of it, the intensity of MitoSOX fluorescence, an indicator of mitochondrial ROS generation, was also attenuated by HA, accompanied by ameliorated post-H/R mitochondrial dysfunction and apoptosis (Fig. 6D–6F). Remarkably, the HA-initiated anti-oxidative and anti-apoptotic effects were absent or blunted when cotreatment the H9c2 cells with DON, indicating the above beneficial effects are O-GlcNAcylation-dependent (Fig. 6A–6F). Together, these results collectively suggested that HA-induced O-GlcNAcylation activates cardiac G6PDH and improves redox homeostasis, which counteracts H/R injury in cardiomyocytes.

### 3.6. HA mitigated cardiac I/R injury via O-GlcNAcylation-mediated antioxidative effect and mitochondrial preservation

To confirm the beneficial effect of HA on the I/R heart is attributed to protein O-GlcNAcylation *in vivo*, we pretreated the HA mice with ALX or TMG for 6 h before I/R surgery (Fig. 7A). As expected, protein O-GlcNAcylation levels in the HA hearts were attenuated by ALX and increased by TMG in comparison with the HA + Veh group (Fig. 7B). Along with the downregulated levels of O-GlcNAcylation, ALX reversed the anti-I/R effect of HA, as evidenced by the increased infarct size and elevated circulating CK-MB levels at 24 h, and the enlarged scar size at 7 days after I/R. By contrast, enhancement of O-GlcNAcylation by TMG further limited the infarct size on top of HA, and maintained the serum CK-MB and scar size at low levels (Fig. 7C–H), suggesting that upregulation of O-GlcNAcylation contributes to HA-initiated cardioprotective

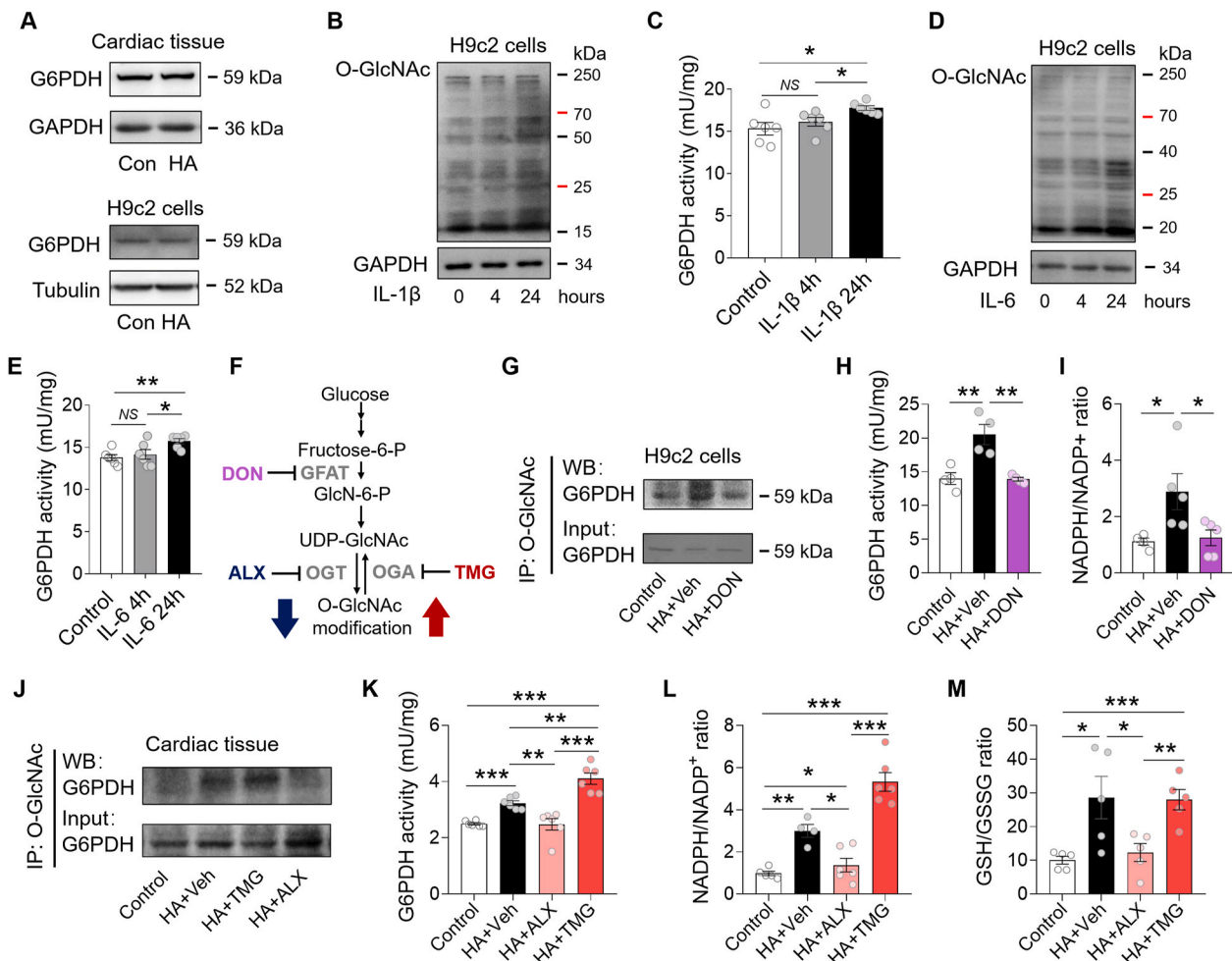


**Fig. 5.** PPP was enhanced via O-GlcNAcylation-mediated activation of G6PDH. **A**, Representative blots of G6PDH in cardiac tissues and H9c2 cells ( $n = 4$  per group). **B–C**, Representative blots of O-GlcNAc modified G6PDH (**B**) and G6PDH activity (**C**) in H9c2 cells treated with IL-1 $\beta$  for 4 or 24 h ( $n = 6$  per group). **D–E**, Representative blots of O-GlcNAc modification (**D**) and the G6PDH activity (**E**) in H9c2 cells treated with IL-6 for 4 or 24 h ( $n = 6$  per group). **F**, The compounds used in this study for targeting HBP pathway enzymes. **G–I**, Representative blots of O-GlcNAc-modified G6PDH (**G**), G6PDH activity (**H**), and NADPH/NADP<sup>+</sup> ratio (**I**) in H9c2 cells with indicated treatments ( $n = 4–5$  per group). **J**, Representative blots of O-GlcNAc modified G6PDH in the mouse hearts with indicated treatments ( $n = 3$  per group). **K–M**, The G6PDH activity (**K**), NADPH/NADP<sup>+</sup> ratio (**L**), and GSH/GSSG ratio (**M**) in the mouse hearts with indicated treatments ( $n = 4–6$  per group). Data are shown as mean  $\pm$  SEM. \* $P < 0.05$ , \*\* $P < 0.01$  and \*\*\* $P < 0.001$  for indicated comparisons. NS: no significant difference.

effect. Moreover, ALX treatment robustly elevated protein carbonylation in the HA hearts after I/R injury, while it persisted at low levels in the HA + Veh and HA + TMG group hearts (Fig. 7I). In addition, in the HA + ALX hearts, we observed a large number of swollen mitochondria with disorganized cristae and less dense matrix, whereas the aberrant mitochondria were much less in the HA + Veh and HA + TMG hearts (Fig. 7J). Seahorse analysis confirmed that ALX abrogated while TMG enhanced HA-induced improvement of mitochondrial respiration, suggesting that the benefits of HA on mitochondrial ultrastructure and function were at least partially mediated by protein O-GlcNAc modification (Fig. 7K). Taken together, these results demonstrated that HA reduces oxidative stress, protects mitochondria, and mitigates cardiac I/R injury through upregulation of O-GlcNAcylation.

#### 4. Discussion

In this study, we demonstrated that HA-associated inflammatory cytokines upregulated HBP pathway and activated G6PDH by increasing the O-GlcNAcylation in the heart. Importantly, such response improved PPP pathway and enhanced redox homeostasis, which alleviated acute I/R injury in mouse hearts and cultured cardiomyocytes (Fig. 8). These findings, therefore, identified HA as a promising anti-I/R strategy for the

heart and proposed O-GlcNAc modification of G6PDH as a therapeutic target in ischemic heart disease.

In physiological conditions, the cellular energy metabolism preferentially relies on oxidative phosphorylation, while during hypoxia, cells shift to a primarily glycolytic phenotype for energetic needs. The increased glycolytic flux is recognized as an adaptive mechanism during hypoxia, such as the “Warburg” effect in cancer cells. Here, we report that HA upregulates HBP and increases O-GlcNAc modification in the heart, resulting in resistance to I/R injury. The HBP is an accessory pathway of glucose metabolism accounting for approximately 5% of glucose entering cells. O-GlcNAc modifications are catalyzed by OGT and removed by OGA, which utilizes UDP-GlcNAc, the final product of the HBP pathway as its substrate. Recent studies suggested that O-GlcNAcylation modulates the function of numerous proteins under both physiological and pathological conditions, emerging as a key mediator of many cardiovascular pathophysiological processes [30–36]. Upregulation of HBP and increased O-GlcNAc modification have been shown to be protective against acute I/R injury in previous studies by ourselves and others [26,37,38]. Because the rescue effect of HA on cardiac I/R injury can be overridden by suppression of O-GlcNAcylation and augmented by promotion of it, our results indicate a causal link between HA-regulated glucose metabolism and stress response in the heart.

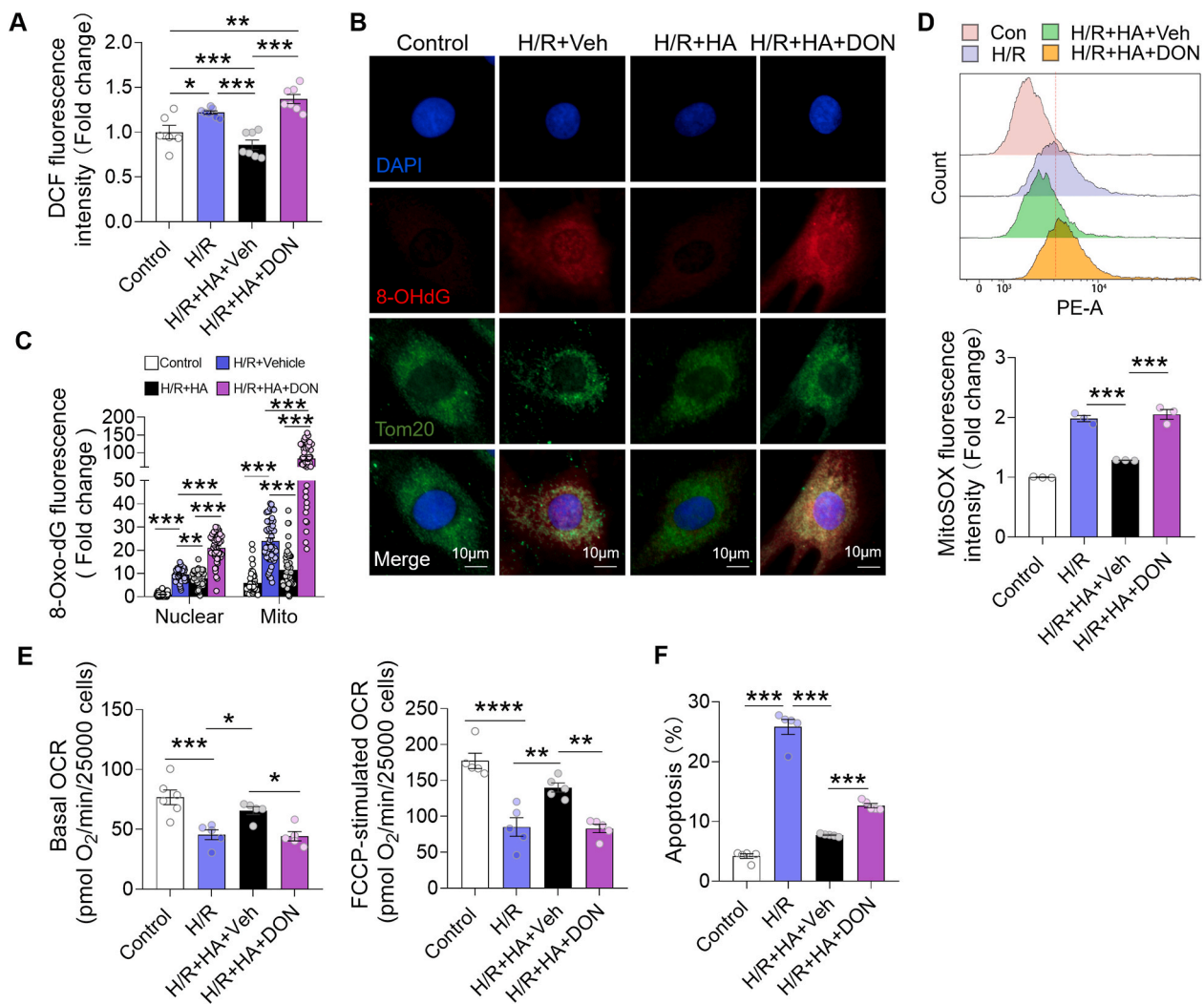


**Fig. 6.** HA attenuated acute oxidative insult in H9c2 cells in an O-GlcNAcylation-dependent manner. **A**, The global cellular reactive oxygen species (ROS) production measured in H9c2 cells measured by CM-H2DCFDA ( $n = 6-7$  per group). **B**, Representative fluorescence images of oxidative DNA damage measured by immunostaining for 8-Oxo-dG (red), nuclei (DAPI; blue) and mitochondria (Tom20; green). Scale bar, 10  $\mu\text{m}$ . **C**, Quantitative analysis of 8-Oxo-dG positive staining in nuclei and mitochondria, and the results were normalized to the intensity in nuclear compartment of the control group ( $n = 50$  cells per group). **D**, The MitoSOX flow cytometry analysis and the fluorescence intensity in H9c2 cells with indicated treatments ( $n = 3$  per group). **E**, The oxygen consumption rates (OCR) of H9c2 cells at baseline and after FCCP stimulation ( $n = 5-6$  per group). **F**, The levels of apoptosis in H9c2 cells with indicated treatments ( $n = 5$  per group). Data are shown as mean  $\pm$  SEM. \* $P < 0.05$ , \*\* $P < 0.01$  and \*\*\* $P < 0.001$  for indicated comparisons. (For interpretation of the references to colour in this figure legend, the reader is referred to the Web version of this article.)

Although O-GlcNAc-mediated cardioprotection is consistently observed in the context of acute injury, the role of O-GlcNAc in the vasculature or in the chronically failing/diabetic heart is ambiguous, for that O-GlcNAcylation is also reported to contribute to insulin resistance and diabetic cardiomyopathy [35,39].

Our findings suggest that HA-evoked inflammation, by promoting HBP and protein O-GlcNAcylation, would be beneficial to cardiac I/R stress. Besides, macrophage migration inhibitory factor (MIF) has been shown to mitigate cardiac I/R injury and its expression is regulated by the transcription factor HIF-1 $\alpha$  [40]. Since the HIF-1 $\alpha$  expression in the HA heart was elevated, it is possible that the HIF-1 $\alpha$ -MIF protective cascade also contributed to the beneficial effects of HA. However, as chronic inflammation is also a potential trigger of cardiac fibrosis and hypertrophy, further mechanistic studies are required to elucidate how this process was precisely controlled under HA conditions.

Glucose does not simply distribute throughout all side branches of glycolysis [41]. We found that before O-GlcNAcylation was upregulated, exposure the H9c2 cells to inflammatory cytokine alone could not activate G6PDH. Further studies showed that reducing O-GlcNAcylation

of G6PDH by DON or ALX blunted the activation effect of HA, and vice versa. Our results, therefore, unveiled a tight coupling of HBP and PPP via O-GlcNAcylation of G6PDH. As a rate-limiting enzyme, G6PDH governs the efficiency of PPP and plays a vital role in cellular redox pathophysiology [29]. The enhanced PPP leads to an increased reduction of NADP<sup>+</sup> to NADPH, and thus increases the cytosol redox potential to drive most ROS clearance mechanisms, among which GSH is one of the most important intracellular antioxidants [42]. GSH is oxidized to GSSG by glutathione peroxidase during detoxification of hydroperoxides, which can be reversed by glutathione reductase using NADPH. Thus, sufficient NADPH and GSH productions are critical in maintaining redox homeostasis and counteracting oxidative stress [43,44]. In line with it, our results showed that HA activates G6PDH and elevates NADPH/NADP<sup>+</sup> and GSH/GSSG couples, which attenuates oxidative stress and mitigates cardiac I/R injury. In addition, G6PDH catalyzes 6-phosphogluconate to ribulose 5-phosphate, which subsequently enters non-oxidative PPP phase and participates in the synthesis of nucleotides and coenzymes. Therefore, activation of G6PDH is also beneficial to generation of nucleotide precursors for cell growth, which may

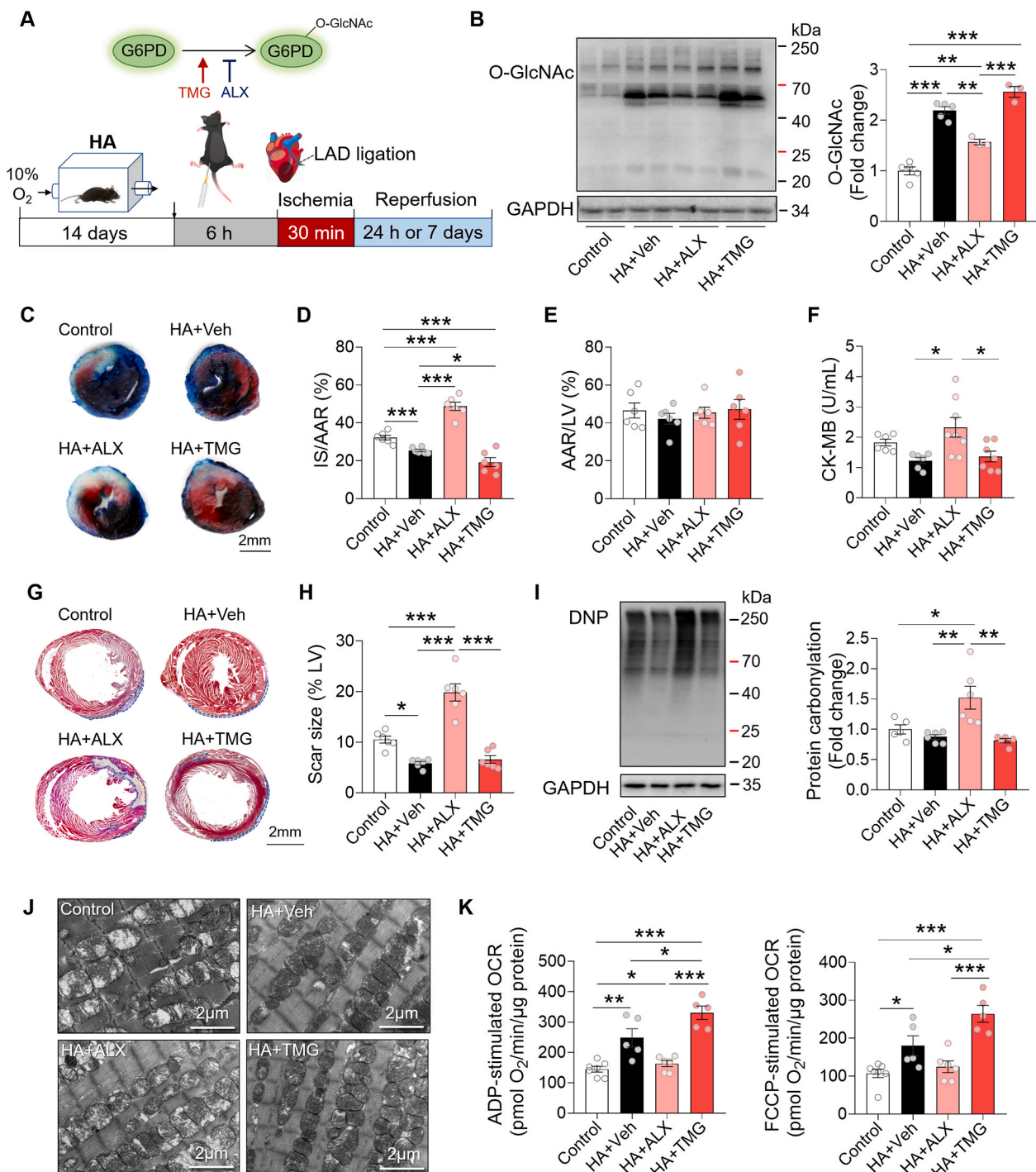


**Fig. 7.** HA mitigated cardiac I/R injury via O-GlcNAcylation-mediated antioxidative effect and mitochondrial preservation. **A**, A schematic representation of the experimental protocol. **B**, Immunoblot analysis of O-GlcNAc modification in the indicated mouse hearts ( $n = 3-5$  per group). **C**, Representative images of Evans blue and TTC double-stained heart sections from Control and HA mice after supplementation of ALX or TMG. Scale bar, 2 mm. **D-E**, Infarct size (IS) relative to area at risk (AAR) (**D**) and AAR relative to left ventricle (LV) (**E**) were quantified ( $n = 6$  per group). **F**, The plasma levels of CK-MB ( $n = 6-8$  per group). **G**, Representative images of Masson's trichrome-stained heart sections 7 days post-I/R. Scale bar, 2 mm. **H**, Quantification of the scar size relative to left ventricle ( $n = 6$  per group). **I**, Representative immunoblots of protein carbonylation in the LV ischemic border zone and quantification of band intensity ( $n = 5-6$  per group). **J**, Representative electron microscopy images of heart sections. Scale bar, 2  $\mu$ m. **K**, The ADP- and FCCP-stimulated oxygen consumption rates (OCR) of the isolated mitochondria from the mouse hearts ( $n = 5-7$  per group). Data are shown as mean  $\pm$  SEM. \* $P < 0.05$ , \*\* $P < 0.01$ , and \*\*\* $P < 0.001$  for indicated comparisons. (For interpretation of the references to colour in this figure legend, the reader is referred to the Web version of this article.)

contribute to the cardiac repair after I/R injury.

In line with a prevailing notion that electron transport chain complexes can adapt to hypoxia by replacing distinct proteins and optimizing the function [45], we found that I/R-induced cardiac mitochondrial dysfunction and aberrant morphology were alleviated by

HA. Besides the improved redox homeostasis, we believe this process is also conducive to attenuating oxidative stress in the I/R heart. Mitochondria are the greatest cellular source of ROS during I/R. Specifically, accumulation of TCA intermediate succinate during ischemia and a reverse electron transport from complex II to complex I during

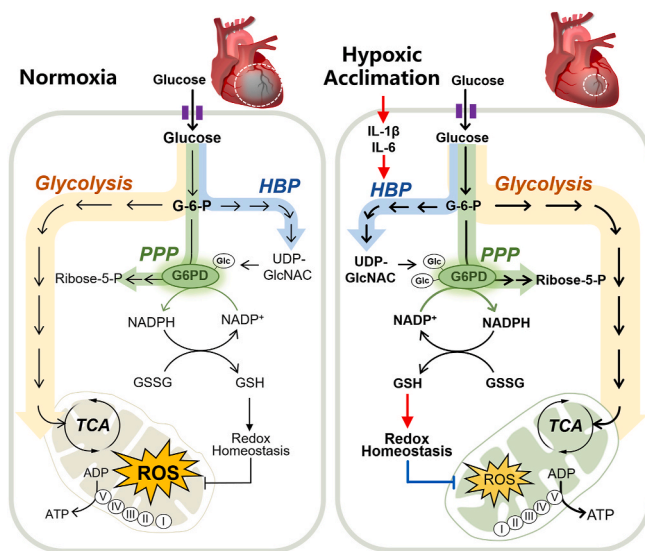


**Fig. 8.** A schematic illustration of the working model of this study. The present study demonstrated that hypoxia acclimation-associated inflammatory cytokines upregulate the hexosamine biosynthetic pathway (HBP) and activate G6PDH by increasing the O-GlcNAcylation, which improves pentose phosphate pathway (PPP)-mediated redox homeostasis, and alleviates acute cardiac I/R injury.

reperfusion could result in a burst of ROS [46]. The increase of ROS together with an I/R-induced calcium ( $\text{Ca}^{2+}$ ) influx into mitochondria opens the mitochondrial permeability transition pore (mPTP), further increase ROS formation, decrease electron transport chain activity, and eventually provoke cell death [47]. Results from the present study show that HA improves succinate-supported mitochondrial respiration, suggesting more efficient succinate catabolism and ATP production in the HA heart. In addition, well organized crista is a prerequisite for super-complex formation, which could repress ROS generation due to the efficiency of electron transfer among complexes [48]. Furthermore, augmenting O-GlcNAcylation of mitochondrial proteins has been reported to prevent excessive formation of mPTP [49], mitigated  $\text{Ca}^{2+}$  overload and ROS generation during I/R injury [39,50]. Therefore, through preservation of mitochondrial ultrastructure and function, HA could suppress ROS overproduction, and thus attenuate I/R-related pathology in the heart.

There are several strengths to our study. We integrated state-of-the-art techniques such as Seahorse mitochondrial analysis and LC-MS/MS based O-glycoproteomics to uncover a protein post-translational modification-regulated redox system in the heart. We also utilized pharmacologic approaches to reveal an O-GlcNAcylation-initiated anti-I/R mechanism *in vivo* and *in vitro*, providing a basis for translation into clinical therapy. We acknowledge that this study has several limitations as well. First, the current data did not address the exact mechanism whereby O-GlcNAcylation activates G6PDH. In our opinion, it could be due to direct activation via O-GlcNAc modification of serine/threonine residues in G6PDH catalytic domain, similar to a recent report about  $\beta$ -OHB-mediated activation of citrate synthase [51], or indirect regulation such as competitive inhibition of other post-translational modification machinery on G6PDH. More detailed studies, like site-specific mutagenesis, are required to test these possibilities. Second, the experiments described here were conducted exclusively in male mice on the C57BL/6J background, and further studies are necessary to check whether HA-initiated beneficial effects have sex and strain differences. Third, the experiments were not fully blinded, despite we followed standard laboratory procedures of randomization and the data were analyzed in a blinded manner.

## 5. Conclusions

In summary, we have demonstrated that HA improves PPP pathway and enhances redox homeostasis through activation of G6PDH, which mitigates cardiac I/R injury *in vitro* and *in vivo*. These findings suggest the interplay between branches of glycolysis as a key driver in the maintenance of redox balance in the I/R heart, and highlight the potential of HA as a simple remedy for ischemic heart disease.

## Declaration of competing interest

The authors declare that they have no known competing financial interests or personal relationships that could have appeared to influence the work reported in this paper.

## Declaration of competing interest

None.

## Acknowledgments

This study was supported in part by grants from the National Key Research and Development Program of China (2020YFC2005601), the National Natural Science Foundation of China (81970715, 81770815, 81801117, 81873500 and 81971806), the Key Research Program of National Clinical Research Center for Geriatrics (Z20191004), the Key Research and Development Program of Sichuan Province (2019YFS0222 and 2019YFS0252), the Innovation Spark Project of Sichuan University (2018SCUH0065), and the 1.3.5 Project for Disciplines of Excellence, West China Hospital, Sichuan University (ZYGD18014). We thank Dr Rongyuan Li, Dr Hanlin Liu, and Chengdu Lilai Biotechnology Co., Ltd for technical assistance in transmission electron microscopy and histological staining.

## References

- [1] G. Heusch, Myocardial ischaemia-reperfusion injury and cardioprotection in perspective, *Nat. Rev. Cardiol.* 17 (2020) 773–789.
- [2] G. Heusch, B.J. Gersh, The pathophysiology of acute myocardial infarction and strategies of protection beyond reperfusion: a continual challenge, *Eur. Heart J.* 38 (2017) 774–784.
- [3] I.Y. Elgendy, D. Mahatta, C.J. Pepine, Medical therapy for heart failure caused by ischemic heart disease, *Circ. Res.* 124 (2019) 1520–1535.
- [4] T. Kalogeris, C.P. Baines, M. Krenz, R.J. Korthuis, Cell biology of ischemia/reperfusion injury, *Int Rev Cell Mol Biol.* 298 (2012) 229–317.
- [5] S.S. Virani, A. Alonso, H.J. Aparicio, E.J. Benjamin, M.S. Bittencourt, C. W. Callaway, A.P. Carson, A.M. Chamberlain, S. Cheng, F.N. Dellinger, M.S.V. Elkind, K.R. Evenson, J.F. Ferguson, D.K. Gupta, S.S. Khan, B.M. Kissela, K.L. Knutson, C. D. Lee, T.T. Lewis, J. Liu, M.S. Loop, P.L. Lutsey, J. Ma, J. Mackey, S.S. Martin, D. B. Matchar, M.E. Mussolino, S.D. Navaneethan, A.M. Perak, G.A. Roth, Z. Samad, G.M. Satou, E.B. Schroeder, S.H. Shah, C.M. Shay, A. Stokes, L.B. VanWagner, N.-Y. Wang, C.W. Tsao, Heart disease and stroke statistics-2021 update: a report from the American heart association, *Circulation* 143 (2021) e254–e743.
- [6] D.M. Yellon, A. Dana, The preconditioning phenomenon: a tool for the scientist or a clinical reality? *Circ. Res.* 87 (2000) 543–550.
- [7] M. Speechly-Dick, M. Mocanu, D. Yellon, Protein kinase C. Its role in ischemic preconditioning in the rat, *Circ. Res.* 75 (1994) 586–590.
- [8] G. Heusch, Molecular basis of cardioprotection: signal transduction in ischemic pre-, post-, and remote conditioning, *Circ. Res.* 116 (2015) 674–699.
- [9] T. Kalogeris, Y. Bao, R.J. Korthuis, Mitochondrial reactive oxygen species: a double edged sword in ischemia/reperfusion vs preconditioning, *Redox Biol* 2 (2014) 702–714.
- [10] J.G. Fariás, V.M. Molina, R.A. Carrasco, A.B. Zepeda, E. Figueroa, P. Letelier, R. L. Castillo, Antioxidant therapeutic strategies for cardiovascular conditions associated with oxidative stress, *Nutrients* 9 (2017) 966.
- [11] C.E. Murry, R.B. Jennings, K.A. Reimer, Preconditioning with ischemia: a delay of lethal cell injury in ischemic myocardium, *Circulation* 74 (1986) 1124–1136.
- [12] D.J. Hausenloy, L. Candilio, R. Evans, C. Ariti, D.P. Jenkins, S. Kolvekar, R. Knight, G. Kunst, C. Laing, J. Nicholas, Remote ischemic preconditioning and outcomes of cardiac surgery, *N. Engl. J. Med.* 373 (2015) 1408–1417.
- [13] X.-L. Liao, X.-X. Hu, F.-J. Chang, H.-Y. Yuan, H.-B. Ci, J.-Y. Wu, Z. Xu, Z.-P. Wang, X. Zhang, Z. Xia, J.-S. Ou, A simple modification results in greater success in the model of coronary artery ligation and myocardial ischemia in mice, *J. Cardiovasc. Pharmacol.* 61 (2013) 430–436.

- [14] M.A. Lui, S. Mahalingam, P. Patel, A.D. Connaty, C.M. Ivy, Z.A. Cheviron, J. F. Storz, G.B. McClelland, G.R. Scott, High-altitude ancestry and hypoxia acclimation have distinct effects on exercise capacity and muscle phenotype in deer mice, *Am. J. Physiol. Regul. Integr. Comp. Physiol.* 308 (2015) R779–R791.
- [15] J.B. West, Physiological effects of chronic hypoxia, *N. Engl. J. Med.* 376 (2017) 1965–1971.
- [16] X. Li, Y. Liu, H. Ma, Y. Guan, Y. Cao, Y. Tian, Y. Zhang, Enhancement of glucose metabolism via PGC-1 $\alpha$  participates in the cardioprotection of chronic intermittent hypobaric hypoxia, *Front. Physiol.* 7 (2016) fphys.2016.00219.
- [17] E.B. Manukhina, L.M. Belkina, O.L. Terekhina, D.V. Abramochkin, E.A. Smirnova, O.P. Budanova, R.T. Mallet, H.F. Downey, Normobaric, intermittent hypoxia conditioning is cardio- and vasoprotective in rats, *Exp. Biol. Med.* 238 (2013) 1413–1420.
- [18] I.H. Jain, L. Zazzeron, R. Goli, K. Alexa, S. Schatzman-Bone, H. Dhillon, O. Goldberger, J. Peng, O. Shalem, N.E. Sanjana, Hypoxia as a therapy for mitochondrial disease, *Science* 352 (2016) 54–61.
- [19] H.R. Griffiths, D. Gao, C. Pararasa, Redox regulation in metabolic programming and inflammation, *Redox Biol* 12 (2017) 50–57.
- [20] M.L. Lindsey, R. Bolli, J.M. Canty Jr., X.-J. Du, N.G. Frangogiannis, S. Frantz, R. G. Gourdie, J.W. Holmes, S.P. Jones, R.A. Kloner, Guidelines for experimental models of myocardial ischemia and infarction, *Am. J. Physiol. Heart Circ. Physiol.* 314 (2018) H812–H838.
- [21] H.E. Botker, D. Hausenloy, I. Andreadou, S. Antonucci, K. Boengler, S.M. Davidson, S. Deshwal, Y. Devaux, F. Di Lisa, M. Di Sante, Practical guidelines for rigor and reproducibility in preclinical and clinical studies on cardioprotection, *Basic Res. Cardiol.* 113 (2018) 39.
- [22] S. Bohl, D.J. Medway, J. Schulz-Menger, J.E. Schneider, S. Neubauer, C.A. Lygate, Refined approach for quantification of in vivo ischemia-reperfusion injury in the mouse heart, *Am. J. Physiol. Heart Circ. Physiol.* 297 (2009) H2054–H2058.
- [23] Y. Liang, X. Xu, Q. Li, Y. Deng, M. Xie, Y. Zheng, W. Ou, Q. He, X. Xu, W. Wu, T. Li, Chronic alcohol intake exacerbates cardiac dysfunction after myocardial infarction, *Alcohol Alcohol* 55 (2020) 524–530.
- [24] O. Lyublinskaya, J.S. Ivanova, N. Pugovkina, I. Kozhukharova, Z. Kovaleva, A. Shatrova, N. Aksenov, V. Zenin, Y.A. Kaulin, I. Gamaley, Redox environment in stem and differentiated cells: a quantitative approach, *Redox Biol* 12 (2017) 758–769.
- [25] J. Leon, K. Sakumi, E. Castillo, Z. Sheng, S. Oka, Y. Nakabeppu, 8-Oxoguanine accumulation in mitochondrial DNA causes mitochondrial dysfunction and impairs neurogenesis in cultured adult mouse cortical neurons under oxidative conditions, *Sci. Rep.* 6 (2016) 22086.
- [26] T. Li, Z. Zhang, S.C. Kolwicz Jr., L. Abell, N.D. Roe, M. Kim, B. Zhou, Y. Cao, J. Ritterhoff, H. Gu, D. Rafferty, H. Sun, R. Tian, Defective branched-chain amino acid catabolism disrupts glucose metabolism and sensitizes the heart to ischemia-reperfusion injury, *Cell Metabol.* 25 (2017) 374–385.
- [27] V. Champattanachai, R.B. Marchase, J.C. Chatham, Glucosamine protects neonatal cardiomyocytes from ischemia-reperfusion injury via increased protein-associated O-GlcNAc, *Am. J. Physiol. Cell Physiol.* 292 (2007) C178–C187.
- [28] S.A. Marsh, H.E. Collins, J.C. Chatham, Protein O-GlcNAcylation and cardiovascular (patho) physiology, *J. Biol. Chem.* 289 (2014) 34449–34456.
- [29] J. Ritterhoff, R. Tian, Metabolism in cardiomyopathy: every substrate matters, *Cardiovasc. Res.* 113 (2017) 411–421.
- [30] N.J. Pedowitz, A.R. Batt, N. Darabedian, M.R. Pratt, MYPT1 O-GlcNAc modification regulates sphingosine-1-phosphate mediated contraction, *Nat. Chem. Biol.* 17 (2021) 169–177.
- [31] K.S. Aulak, J.W. Barnes, L. Tian, N.E. Mellor, M.M. Haque, B. Willard, L. Li, S. C. Comhair, D.J. Stuehr, R.A. Dweik, Specific O-GlcNAc modification at Ser-615 modulates eNOS function, *Redox Biol* 36 (2020) 101625.
- [32] G.A. Ngoh, H.T. Facundo, A. Zafir, S.P. Jones, O-GlcNAc signaling in the cardiovascular system, *Circ. Res.* 107 (2010) 171–185.
- [33] Y.-L. Shiou, H.-T. Lin, L.-Y. Ke, B.-N. Wu, S.-J. Shin, C.-H. Chen, W.-C. Tsai, C.-S. Chu, H.-C. Lee, Very low-density lipoproteins of metabolic syndrome modulates STIM1, suppresses store-operated calcium entry, and deranges Myofilament proteins in atrial Myocytes, *J. Clin. Med.* 8 (2019) 881.
- [34] D.E. Lee, S.J. Lee, S.J. Kim, H.-S. Lee, O.-S. Kwon, Curcumin ameliorates nonalcoholic fatty liver disease through inhibition of O-GlcNAcylation, *Nutrients* 11 (2019) 2702.
- [35] S. Dassanayaka, S.P. Jones, O-GlcNAc and the cardiovascular system, *Pharmacol. Ther.* 142 (2014) 62–71.
- [36] J.C. Chatham, R.B. Marchase, Protein O-GlcNAcylation: a critical regulator of the cellular response to stress, *Curr. Signal Transduct. Ther.* 5 (2010) 49–59.
- [37] Z.V. Wang, Y. Deng, N. Gao, Z. Pedrozo, D.L. Li, C.R. Morales, A. Criollo, X. Luo, W. Tan, N. Jiang, Spliced X-box binding protein 1 couples the unfolded protein response to hexosamine biosynthetic pathway, *Cell* 156 (2014) 1179–1192.
- [38] R. Cong, L. Sun, J. Yang, H. Cui, X. Ji, J. Zhu, J.-h. Gu, B. He, Protein O-GlcNAcylation alleviates small intestinal injury induced by ischemia-reperfusion and oxygen-glucose deprivation, *Biomed. Pharmacother.* 138 (2021) 111477.
- [39] J.N. Wright, H.E. Collins, A.R. Wende, J.C. Chatham, O-GlcNAcylation and cardiovascular disease, *Biochem. Soc. Trans.* 45 (2017) 545–553.
- [40] J. Pohl, U.B. Hendgen-Cotta, P. Stock, P. Luedike, H.A. Baba, M. Kamler, T. Rassaf, Myocardial expression of macrophage migration inhibitory factor in patients with heart failure, *J. Clin. Med.* 6 (2017) 95.
- [41] J.R. Krycer, K. Yugi, A. Hirayama, D.J. Fazakerley, L.-E. Quek, R. Scalzo, S. Ohno, M.P. Hodson, S. Ikeda, F. Shoji, Dynamic metabolomics reveals that insulin primes the adipocyte for glucose metabolism, *Cell Rep.* 21 (2017) 3536–3547.
- [42] D.E. Handy, J. Loscalzo, Responses to reductive stress in the cardiovascular system, *Free Radic. Biol. Med.* 109 (2017) 114–124.
- [43] S. Nóbrega-Pereira, P.J. Fernandez-Marcos, T. Brioché, M.C. Gomez-Cabrera, A. Salvador-Pascual, J.M. Flores, J. Viña, M. Serrano, G6PD protects from oxidative damage and improves healthspan in mice, *Nat. Commun.* 7 (2016) 10894.
- [44] M. Jain, L. Cui, D.A. Brenner, B. Wang, D.E. Handy, J.A. Leopold, J. Loscalzo, C. S. Apstein, R. Liao, Increased myocardial dysfunction after ischemia-reperfusion in mice lacking glucose-6-phosphate dehydrogenase, *Circulation* 109 (2004) 898–903.
- [45] D.C. Fuhrmann, B. Brüne, Mitochondrial composition and function under the control of hypoxia, *Redox Biol* 12 (2017) 208–215.
- [46] E.T. Chouchani, V.R. Pell, E. Gaude, D. Aksentijević, S.Y. Sundier, E.L. Robb, A. Logan, S.M. Nadtochiy, E.N. Ord, A.C. Smith, Ischaemic accumulation of succinate controls reperfusion injury through mitochondrial ROS, *Nature* 515 (2014) 431–435.
- [47] S. Cadenas, ROS and redox signaling in myocardial ischemia-reperfusion injury and cardioprotection, *Free Radic. Biol. Med.* 117 (2018) 76–89.
- [48] D. Milenkovic, J.N. Blaza, N.-G. Larsson, J. Hirst, The enigma of the respiratory chain supercomplex, *Cell Metabol.* 25 (2017) 765–776.
- [49] G.A. Ngoh, L.J. Watson, H.T. Facundo, W. Dillmann, S.P. Jones, Non-canonical glycosyltransferase modulates post-hypoxic cardiac myocyte death and mitochondrial permeability transition, *J. Mol. Cell. Cardiol.* 45 (2008) 313–325.
- [50] G.A. Ngoh, L.J. Watson, H.T. Facundo, S.P. Jones, Augmented O-GlcNAc signaling attenuates oxidative stress and calcium overload in cardiomyocytes, *Amino Acids* 40 (2011) 895–911.
- [51] Y. Deng, M. Xie, Q. Li, X. Xu, W. Ou, Y. Zhang, H. Xiao, H. Yu, Y. Zheng, Y. Liang, C. Jiang, G. Chen, D. Du, W. Zheng, S. Wang, M. Gong, Y. Chen, R. Tian, T. Li, Targeting mitochondria-inflammation circuit by  $\beta$ -hydroxybutyrate mitigates HFpEF, *Circ. Res.* 128 (2021) 232–245.